Quantitative measurement of hydroxyl radical (OH) concentration in premixed flat flame by combining laser-induced fluorescence and direct absorption spectroscopy*

Shuang Chen(陈爽)[1,2,†], Tie Su(苏铁)[2], Zhong-Shan Li(李中山)[3], Han-Chen Bai(白菡尘)[1,2], Bo Yan(闫博)[2], and Fu-Rong Yang(杨富荣)[1,2]

[1] *Science and Technology on Scramjet Laboratory, Hypervelocity Aerodynamics Institute of China Aerodynamic Research and Development Center, Mianyang* 621000, *China*

[2] *China Aerodynamics Research and Development Center, Mianyang* 621000, *China*

[3] *Division of Combustion Physics, Lund University, P. O. Box* 118, 22100 *Lund, Sweden*

(Received 28 March 2016; revised manuscript received 23 June 2016; published online 25 August 2016)

An accurate and reasonable technique combining direct absorption spectroscopy and laser-induced fluorescence (LIF) methods is developed to quantitatively measure the concentrations of hydroxyl in CH_4/air flat laminar flame. In our approach, particular attention is paid to the linear laser-induced fluorescence and absorption processes, and experimental details as well. Through measuring the temperature, LIF signal distribution and integrated absorption, spatially absolute OH concentrations profiles are successfully resolved. These experimental results are then compared with the numerical simulation. It is proved that the good quality of the results implies that this method is suitable for calibrating the OH-PLIF measurement in a practical combustor.

Keywords: laser-induced fluorescence (LIF), direct absorption spectroscopy, hydroxyl radical (OH), quantitative measurement

PACS: 07.60.Rd, 33.80.–b, 42.62.–b, 42.62.Fi **DOI:** 10.1088/1674-1056/25/10/100701

1. Introduction

Laser induced fluorescence (LIF) has been playing an increasing role in combustion research over the last 20 to 30 years. It is the best method for measuring OH radical, the important intermediates in combustion processes, with high sensitivity, high temporal and spatial resolution.[1–3]

Unfortunately, in the LIF measurement, the induced fluorescence signal density captured by the intensify-CCD or PMT is not only dependent on the absolute concentration of the species excited by the laser pulse, but also related to other processes such as electronic quenching, vibrational energy transfer (VET), and rotational energy transfer (RET).[4–6] These processes are mainly influenced by many components such as the molecular collisional partner, pressure, temperature and quantum state. Therefore, LIF measurement for quantitative species concentration becomes complex and uncertain, especially in such quasi-practical combustors as a gas turbine, engine and other industry facilities.[7] Thus, it is necessary to find some supplementary techniques and calibration methods for the quantitative OH–LIF measurement. Although the direct absorption is undoubtedly an independent measurement skill for detecting absolute molecular concentrations,[8–11] it has been shown that this technique is of low spatial revolution in the non-uniformity field. Therefore, combining LIF and direct absorption is the feasible method to solve the problems mentioned above.

Our present investigation is based on some recent researches,[12–14] which gives the detailed OH information of typical flames to analyze and understand the flame structure and burning velocity in laminar and turbulent flames. But, only relevant OH–PLIF imaging was acquired in these researches. Hence, a strategy for measuring the quantitative OH concentration in the flame is useful and could play an important role in this field.

In our work, we build an accurate experimental system by combining the direct absorption and LIF methods to measure the absolute concentration of hydroxyl in a flat laminar flame (a McKenna sintered bronze burner) under known conditions. On this basis, we analyze the mechanisms of linear laser-induced fluorescence and direct absorption and try to find an effective method of determining the absolute density. In our approach, more detailed factors are taken into account in both experiment and measurement.

The rest of this paper is organized as follows. In Section 2 we elaborate on the method and experimental setup in combination with LIF and direct absorption spectroscopy methods. Experimental results and a discussion are shown in Section 3. Conclusions are drawn in Section 4.

*Project supported by the National Natural Science Foundation of China (Grant No. 11272338), the Science and Technology on Scramjet Key Laboratory Funding, China (Grant No. STSKFKT 2013004), and the China Scholarship Council.

†Corresponding author. E-mail: chenshuang827@gmail.com

© 2016 Chinese Physical Society and IOP Publishing Ltd

2. Quantitative measurement method

2.1. Experiment setup

The flame in the study is a methane/air flat flame, stable on a water-cooled sinter burner (McKenna). In combination with a 6-cm diameter stainless steel disk and a nitrogen shroud, the combustion products can be prevented from being mixed with the surrounding air.[15] A series of calibrated Bronkhorst mass flow meters is used to measure and control the flow rate of methane and air. The measuring location is selected at 15 mm above the burner plate for the good optical access and negligible temperature gradients around this point indicated in the work of the German Aerospace Center (DLR).[16]

The optical setup is shown in Fig. 1. In the laser system, a tuneable dye laser (Cobra Stretch-G-2400, Sirah) pumped by a 532 nm laser beam from Nd:YAG (Quantra Pro 250-10) is used. The $Q_1(6)$ rotational line in the $A^2\Sigma^+$–$X^2\Pi(0,0)$ band of OH around 309 nm is chosen as the absorption and excitation line for its low-dependence on temperature and strong absorption coefficient.

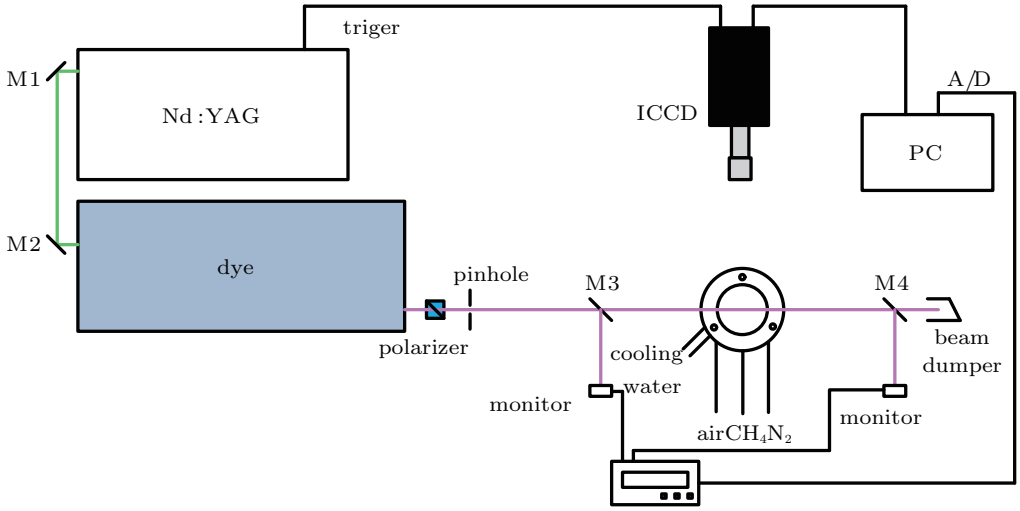


Fig. 1. (color online) Schematic diagram of the diagnostic system for LIF and direct absorption.

Based on the mechanism of LIF, the relation between local laser and fluorescence intensities is variable and nonlinear with increasing laser energy as a result of saturation phenomena. Thus, the key to this experiment is to maintain the linear regime. Then, a laser beam with the sufficiently lower energy pulse is required and weakened by a polarizing prism.

No lens can organize the laser sheet to acquire planar measurement since the absorption behavior is more obvious in a laser beam than in a laser sheet. So, the laser beam with the diameter of less than 2.5 mm is selected due to the pinhole.

The laser beam is achieved by frequency doubling the dye laser output. The dye used is Rhodamine 640 and the wavelength is tuned to the peak of the $Q_1(6)$ resonance of OH at 308.79 nm. The fluorescence signal is captured by a PI-MAX1 ICCD (512×512 pixels) using an UV lens with 100-mm focal length (B. Halle); there is no filter arranged beyond ICCD because the absorption and emission band ($A^2\Sigma^+$–$X^2\Pi(0,0)$) are identical. Moreover, it is noted that the image signal consists of fluorescence, background and Rayleigh scattering.

A shorter gating (less than 100 ns) of the CCD intensifier is used to suppress the undesired background from scattered laser light in both the laboratory and the flame emission. Otherwise, the signal of Rayleigh scattering is difficult to be removed by optical and temporal filters. In our case, we choose a calibrated strategy to solve this problem. The original fluorescence signal and pure Rayleigh scattering signal are captured separately by the same laser pulse energy and the different laser wavelengths under the same flame condition. During this processing, the laser wavelength needs to be adjusted to mismatch the excitation line without inducing the fluorescence. Then the real fluorescence signal is obtained by the minus processing between these two types of images.

In order to measure the laser light attenuation, pyroelectric joulesmeters (Laser Probe, Rm-3700 Universal Radiometer with Rjp-435 Pyroelectric Energy Probe) are used to monitor the laser energy before and after passing the flame. The output signal is from the real-timely sampled voltage probe (Tektronix P6015A) and transformed into digital data. The LIF profile is a superimposition of the measurements of over hundreds of laser shots.

2.2. Combined method approach

The principles and theories of OH–LIF measurement can be found in Ref. [17], so only a brief description is given here. The number of fluorescent photons per unit of time captured by the photodetectors such as PMT and ICCD, S_f, can be ex-

pressed as follows:

$$S_{\rm f} = \frac{G \cdot \Omega \cdot V}{4\Pi} h\nu_{\rm f} N_{\rm p}, \quad (1)$$

where G is the gain of the optical collection system, Ω is the solid angle of collection in unit sr, and V is the probe volume in unit m^3. In spite of the setup and optical layout which is easy to be calibrated and controlled, $S_{\rm f}$ depends on the local fluorescent photon number density $N_{\rm p}$. As indicated in the experimental setup and coordinate system shown in Fig. 1, a laser beam traverses the flame from the left ($x = 0$) to the right ($x = L$). The fluorescence intensity in a linear regime at point x is simply expressed as follows:

$$F(x) = \beta \cdot B_{12} \cdot \frac{h}{\lambda} \cdot f_{\rm B}(T,x) \cdot \eta_{\rm f}(x) \cdot \phi(x) \cdot N_{\rm OH}(x) \cdot I(x), \quad (2)$$

where $I(x)$ is the laser intensity at position x, $N_{\rm OH}(x)$ is the number density of hydroxyl radical, β is a proportionality factor, which is determined by the efficiency of the collecting optics. B_{12} is the Einstein absorption coefficient. $f_{\rm B}$ and $\eta(x)$ are the Boltzmann fractions in the initial quantum state and the fluorescence quantum yield respectively. The former is only dependent on the temperature for a certain transition; the latter is determined not only by the temperature, but also by the pressure. The local spectral overlap integral $\phi(x)$ can be expressed in function (3), where $g_{\rm L}$ and $g_{\rm a}$ are normalized line shape distributions of the laser and the corresponding absorption line.

$$\phi(x) = \int_0^{\infty} g_{\rm L}(x,\nu) g_{\rm a}(\nu) \, {\rm d}\nu. \quad (3)$$

For the absorption in the LIF processing, the attenuation of the laser density is governed the Lambert–Beer law:

$$-\frac{{\rm d}I(x)}{{\rm d}x} = \alpha(x) I(x), \quad (4)$$

where α is the absorption coefficient and $I(x)$ is the laser intensity at position x. The absorber is a hydroxyl radical and the Lambert–Beer law is transformed into

$$-\frac{{\rm d}I(x)}{{\rm d}x} = -I(x) \cdot N_{\rm OH}(x) \cdot \sigma_{\rm total} \cdot f_{\rm B}(T,x) \cdot \phi(x), \quad (5)$$

where $\sigma_{\rm total}$ is related to the Einstein coefficient B_{12}, named total absorption cross section, and it is independent of $f_{\rm B}$ and overlap integral $\phi(x)$.

It needs to be figured out whether the relation function (3) holds true in a linear regime,[9] which can be indicated in the measurement results of the fluorescence distributions and intensities at different laser pulse energies shown in Fig. 2.

It is clear that the relation between fluorescence and laser energy is exactly linear only in lower regime (see Fig. 2(a)). The laser energy needs to be adjusted until it is lower than 0.5 mJ to keep the LIF signal in a linear regime in our experiment. The other interesting phenomenon is the normalized fluorescence density distributions which are normalized from 0 to 1. The plots indicate the relevant fluorescences with changing the laser pulse energies from 0.01 mJ to 1.5 mJ. There are some differences along the laser path (from the left side to the right side of the burner), especially at the ends of some identical flame (see Fig. 2(b)).

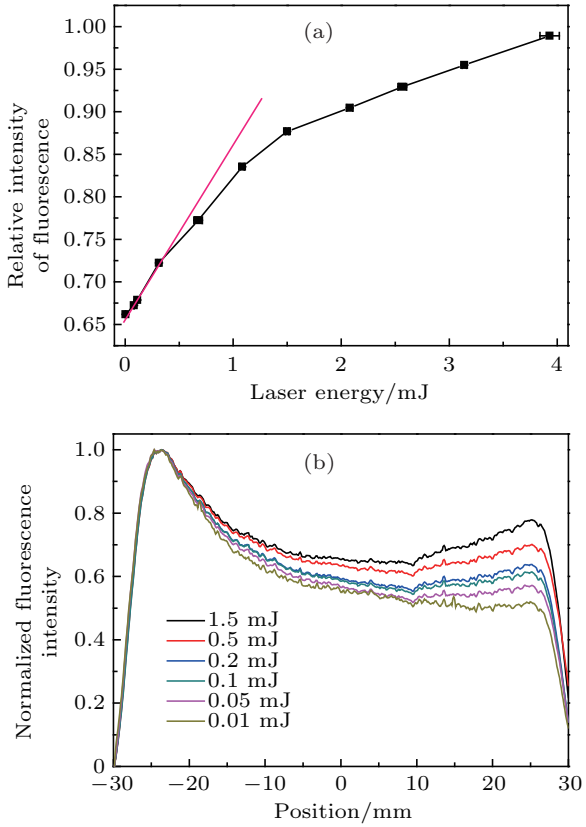


Fig. 2. (color online) Fluorescence distribution and laser pulse energies in LIF.

Since the saturation of the LIF process in the higher laser pulse is so heavy, no obvious decay of fluorescence is found along the laser propagating direction. Thus, in all the cases of our present work, the laser intensity needs to be attenuated to ensure that the excitation transition is not saturated and the LIF intensity is linear with laser power. In our case, the limited energy of the laser pulse is 50 μJ based on the experiment results.

The other interesting thing is that the absorption can change the lineshape (spectral distribution) of the laser and the overlap integral $\phi(x)$, further influencing the relationship between $I(x)$ and $F(x)$, especially in using the laser with a broader bandwidth. The distortion of laser shape can be calculated from the following function:

$$g_{\rm L}(x,\nu) = g_{\rm L}(0,\nu) \exp\left(-\int_0^x \alpha(x',\nu) \, {\rm d}x'\right). \quad (6)$$

Numerical results are used to illustrate this behavior as shown in Fig. 3. The inset shows the spectral change of

laser line for an example (FWHM of laser is 0.3 cm^{-1}, line is $Q_1(6)(0–0)$, $N_{OH} = 1 \times 10^{18}$ cm^{-3}). A significant portion of the radiation is absorbed near the center frequency, where the overlap with the molecular line shape is high, and the wings of the profile are almost unaffected. However, it can be found from the calculation that the relationship between ratio $\phi(x)/\phi(0)$ and $I(x)/I(0)$ is not dependent on the concentration of OH nor laser pulse energy but the shape of laser line. Consequently, in terms of the relation mentioned above, it is feasible to solve the absolute density in the present work in a certain laser system.

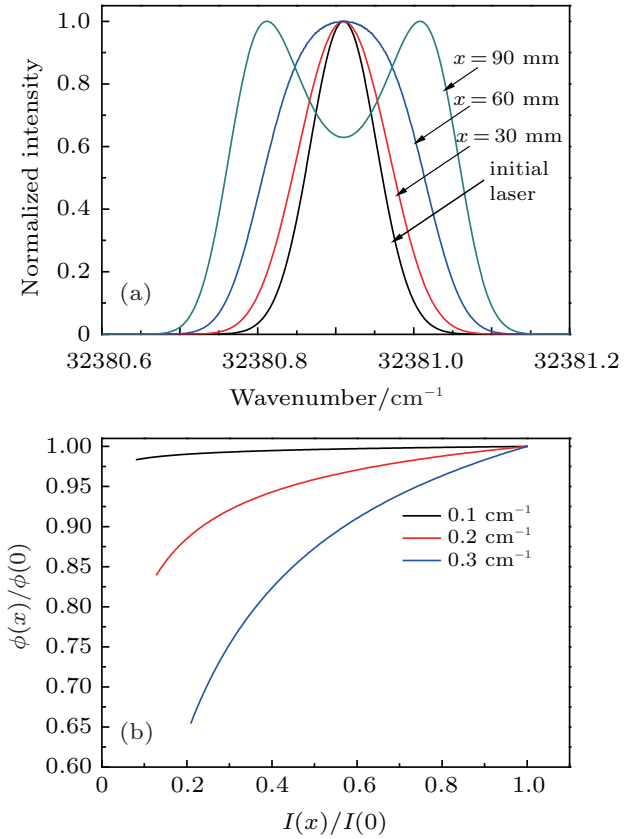


Fig. 3. (color online) Laser lineshape distributions.

Under linear excitation conditions, equation (4) can be transformed into

$$-\frac{\mathrm{d}I(x)}{\mathrm{d}x} = -\beta\frac{F(x)}{\eta(x)}. \tag{7}$$

The quantum yield $\eta(x)$ is determined by several collisional effects, such as collision, pressure, electronic quenching, rotational energy transfer (RET) and vibrational energy transfer (VET); these effects are mainly due to pressure. In the present work, all the flame cases are measured at the atmosphere, then the yield is constant at each position along the optical path. Under this assumption, the integration of Eq. (4) for $I(x)$ yields

$$-\frac{I(x)}{I(0)} = 1 - C\int_0^x F(x)\,\mathrm{d}x, \tag{8}$$

where C is the integration constant. Thus we find the relation between the initial laser energy and the fluorescence intensity distribution. At position x, C could be calculated out by the in/out energy ratio $I(L)/I(0)$, which is monitored by the joulesmeters. To obtain the absolute density of OH, it is necessary to determine the normalized overlap integral $\phi(x)$ and Boltzmann fraction f_B in Eq. (6) based on Beer–Lambert's law. Therefore, as mentioned before, the ratio $\phi(x)/\phi(0)$, which has a certain relation to $I(x)/I(0)$, could be determined directly by looking up the table such as the one indicated in Fig. 3(b). It is noted that the molecular line shape of OH can be approximately regarded as being constant in a temperature range of 1500 K–2200 K of interest under the atmosphere pressure. In this work, the absorption line shape is regarded as a Voigt profile, which consists of the Lorentzian profile and the Gaussian one. These two profiles rely on collisional broadening and Doppler broadening respectively. The line shape of the laser is assumed to be a Gaussian distribution with a full width at half maximum of 0.1 cm^{-1}. Another key point f_B is the Boltzmann fraction values at different positions, which are mainly influenced by temperature. Since the temperature value at the same height above the burner can be taken to be the same in the cases of typical McKenna flame, f_B is independent of position x. So we use a thermocouple detector to measure the temperature in our experiment and the f_B value is calculated based on Ref. [18] and the datasheet from LIFBase.[19]

In order to gain more accuracy in the parameters of a certain flame to further study the quenching behavior of OH–LIF, we choose 11 cases which are listed in Table 1 to compare with the DLR work.[18] The probe position is located on the burner axis at $h = 15$ nm above the burner plate, and Φ is the equivalent ratio determined by flow rates.

For these typical flames, a series of single-pulse CARS spectra is measured in Ref. [16] (see T in Table 1), and a long time thermocouple detector is used in this work (see T^* in Table 1). Obviously, the measured temperature T is lower than the temperature T^* in Ref. [16] because of the heat radiation of the thermocouple. But the gaps are near 250 K and overall results are roughly in line with the trend of CARS. Therefore, the CARS temperature is more accurate and is used to determine the concentration of OH.

The fluorescence signal is measured at the temporal peak of fluorescence and the measurements are averaged over 200 laser pulses. The initial laser pulses are lower than 500 μJ to keep LIF in a linear regime. Two typical images of fluorescence signal are shown in Fig. 4, where the left and right ones are corresponding to CH_4/air flame Case 8 (E.R.=1.0) and Case 11 (E.R.=1.2). The diameter of laser beam is less than 2.5 mm, and the spatial energy distribution of laser beam can be regarded as being uniform.

Table 1. Flow conditions and temperature measurements in atmospheric Methane–Air flame.

Flame case	Φ	CH_4 [slpm]	Air [slpm]	T^*/K (CARS result from [x])	T/K (thermocouple measured)	C-number/10^{-10} (measured)
1	0.7	1.1	15	1706	1465	8.41928
2	0.8	1.31	15.6	1765	1502	8.90251
3	1	1.31	12.4	1790	1527	10.3521
4	1.1	1.31	11.31	1754	1438	10.3354
5	1.2	1.31	10.4	1723	1469	9.40472
6	0.9	1.42	15	1799	1516	9.95778
7	0.8	1.733	20.63	1828	1579	9.61952
8	1	1.733	16.5	1886	1605	10.1029
9	1.1	1.735	15	1818	1547	9.45027
10	1.2	1.733	13.7	1828	1531	8.71226
11	1.4	1.733	11.8	1813	1576	7.27621

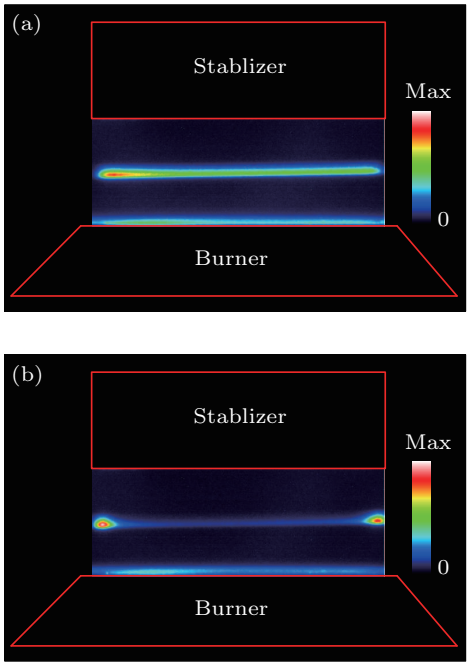


Fig. 4. (color online) Typical original images of laser-induced fluorescence in Cases 3 and 8 introduced in Table 1.

All the images are then post-processed using a homemade Matlab program to extract the relative OH concentration radial profiles in the burned gases. Based on these processed images of OH–LIF signal, the local relevant fluorescence distributions $F(x)$ of the 11 cases can be detected and then smoothed by the Savitzky–Golay method as shown in Fig. 5(a). It is noticed that the nonsymmetrical characteristics of LIF results validate the attenuation of laser energy along the beam path. These results are due to absorption.

The ratio of local laser intensity to initial energy $I(x)/I(0)$ is calculated. Then, the C-number in Eq. (8), which is listed in Table 1, is measured from the in/out energy ratio $I(L)/I(0)$. To obtain the absolute density of OH, it is necessary to determine the normalized overlap integral $\phi(x)$ and Boltzmann fraction f_B in Eq. (6) based on Beer–Lambert's law.

Finally, the concentration of OH (local number density) is obtained using the function (9) as shown in Fig. 5(b). Another important coefficient σ_{total} (total absorption cross section), which has been mentioned in Eq. (6), is acquired from the LifBase database[19] and our work (Ref. [20]).

$$N(x) = \frac{-\ln[(I(x+\Delta x))/I(x)]}{(\sigma_{total} \cdot f_B(T,x) \cdot \Delta x)}. \tag{9}$$

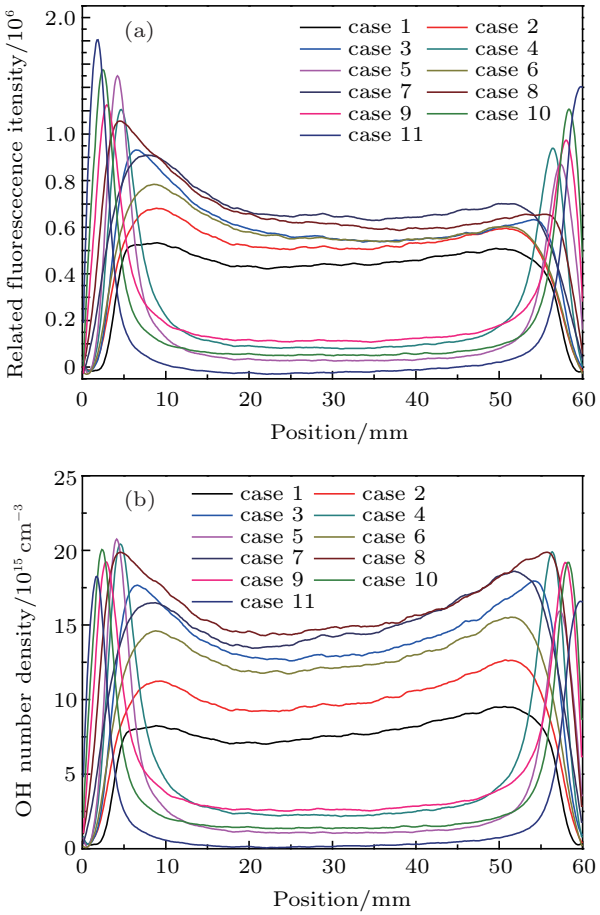


Fig. 5. (color online) Fluorescence distributions and measured concentration profiles of OH.

In Fig. 3 the experimental OH fluorescence distributions are compared and OH concentration profiles are calculated in the premixed CH_4/air flames. It can be observed that the OH profile tends to be U-shaped due to the OH consumption in the burned gases, especially in rich flames. The maximum value of OH concentration is indicated in stoichiometric flames. The concentrations of OH along a line from different cases are in accordance with those of these expected types of flames of the

McKenna burner. It is worth noting that the OH concentration should be a fixed value in the horizontal direction in spite of the boundary performance. But the measured concentration distribution obviously presents a rise-slope shape in lean flames. This is because of some error sources in the measurement, which will be discussed later. The special concentrations in an about 40 mm-long inner linear range are more reliable and can be compared with the numerical simulation using the PREMIX code.[21]

3. Results and discussion

The average OH concentrations in the separate cases are shown in Fig. 6. The region is 15 mm above the burner. It is worth noting that we use the data of the central area (from −20 mm to 20 mm) to acquire the average OH concentration in the present work. Because the wing-like structure of the OH concentration and temperature distributions are typical for this burner, only the results in the central area could be considered to compare with the simulation. The measured average OH concentration varies from E.R. = 0.7 to 1.4. A peak appears at the stoichiometric ratio. Considering the different practical conditions from an adiabatic flame, we find the tendencies of measurements and calculations to be well consistent with each other. It is also clear that the measured concentrations are higher than calculated ones of a lean and stoichiometric flame, and the opposite behavior for a rich flame (see Fig. 6(a)). One reason is that the potential error results from the measuring of laser pulse energies; therefore there could be a big gap between the practical measurement and the simulation in the case of an adiabatic flame.

Figure 6(b) shows the relation between average fluorescence intensity and measured concentration of OH radical in the middle area. The quantum efficiency in the LIF process can then be calculated easily. An approximately linear relationship can be achieved as indicated by the slope in Fig. 6(b) as we expected. The yields of cases 6 and 8 are less than those in other cases, and they can be possibly explained by high collisional quenching induced by CO_2 in the measurement zone.[16]

For all of these experiments, the uncertainty of the OH concentration distribution measurement mainly comes from two parts: the experiment setup and the spectral assumption about absorption and the LIF process. The biggest one is the error from fluorescence trapping, which is determined by the optical system and the response of the ICCD. Secondly, we ignore the temperature falls of about 200 K–400 K at the edge of the burner. This difference brings some errors to the Boltzmann fraction.

The absolute uncertainty of the equivalence ratio is ±2%, determined by a careful calibration of each flow-meter realized in our laboratory. The uncertainty of the temperature in calculation (about ±2.5%) is cited from the literature. Meanwhile, the approximation of equal temperature along the laser absorption path induces bigger error, with an absolute uncertainty of about ±5%.

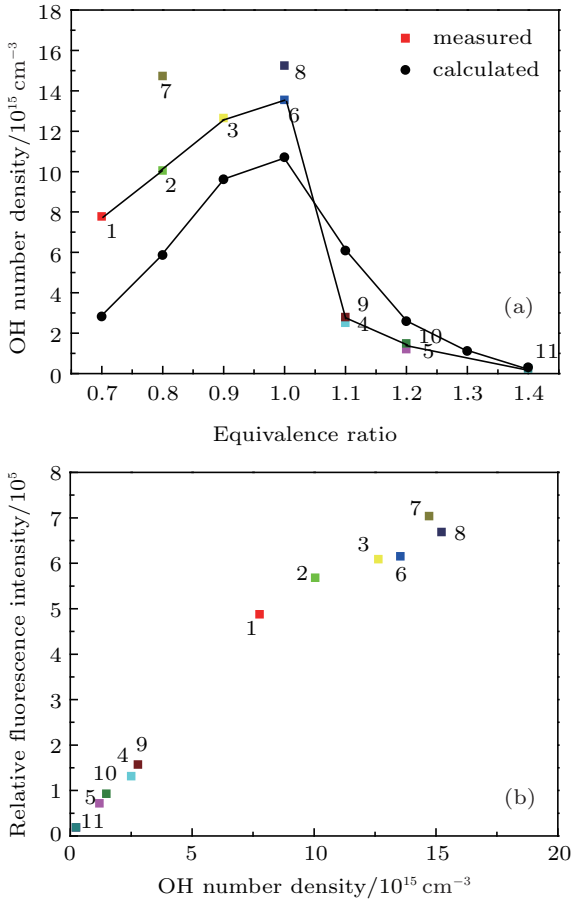


Fig. 6. (color online) Measured average OH concentrations in different cases and numerical results at different equivalence ratios.

The uncertainty of LIF measurements is estimated to be about ±8% with considering the fluorescence trapping error. One uncertainty of the practical absorption measurement is ±10%. Another uncertainty is from spectroscopy, Boltzmann fraction (±2%), and the overlap from the absorption line and laser line (±5%).

Besides, a big error from the temperature and OH concentration distribution falls at the edges (wing-like structure), is estimated at ±5%. The depth of parallelism between the laser beam and the top surface of the burner causes some errors because it could lead to the uncertainty of the optical length. Therefore, we try our best to keep the beam parallel to the burner and then ignore the possible minute error when processing the results.

Consequently, the uncertainty of OH concentration profiles reaches ±25% in the present work.

4. Conclusions

An experimental setup is constructed to measure the absolute concentration of hydroxyl in a CH_4/air flat laminar flame

(McKenna sintered bronze burner). A reasonable technique combining direct absorption spectroscopy and LIF methods is developed to quantitatively measure the concentrations of hydroxyl in different flame cases. Particular attention is paid to the linear laser-induced fluorescence, absorption and excitement processes of hydroxyl. In our approach, more details of the experimentally measured signal of OH concentration were taken into account as much as possible. On this basis, the temperature, LIF signal distribution and integrated absorption are measured to determine the absolute concentrations. The technique is successfully used to determine spatially resolved absolute OH concentrations at an equivalence ratio from 0.7 to 1.4. The results are compared with the calculation and the relation between fluorescence and absolute concentration of OH is discussed in this work.

The good quality and reliability of the results demonstrate the ability of the technique to measure species profiles as a calibration method of quantitative measurement in a practical combustor using LIF. Finally, it is important to emphasize that potential error sources and approaches still affect the accuracy in measuring and post-processing, especially in the high pressure environment. The next step of this study is to achieve the quantitative measurement of hydroxyl in elevated pressure flames, and investigate the collisional fluorescence quenching. This topic will be disccussed in future work.

References

[1] Seitzman J M and Hanson R K 1993 *Planar Fluorescence Imaging in Gases* (London: Academic Press)

[2] Lee M P, McMillin B K, Palmer J L and Hanson R K 1992 *J. Propulsion Power* **8** 729

[3] Han Y, Cai G B, Xu X, Renou B and Boukhalfa A 2014 *Chin. Phys. B* **23** 058901

[4] Kohse-Höinghaus K 1994 *Prog. Energy Combust. Sci.* **20** 203

[5] Paul P H 1994 *J. Quantum Spectrosc. Radiat. Transfer* **51** 511

[6] Bailey A E, Heard D E, Henderson D A and Paul P H 1999 *Chem. Phys. Lett.* **302** 132

[7] Chen S, Su T, Yang F R, Zhang L and Zheng Y B 2013 *Chin. Opt. Lett.* **11** 053001

[8] Arnold A, Bombach R, Käppeli B and Schlegel A 1997 *Appl. Phys. B* **64** 579

[9] Versluis M, Georgiev N, Martinsson L, Alden M and Kroll S 1997 *Appl. Phys. B* **65** 411

[10] Matynia A, Idir M, Molet J, Roche C, de Persis S and Pillier L 2012 *Appl. Phys. B* **108** 393

[11] Yu X, Yang Z, Peng J B, Zhang L, Ma Y F, Yang C B, Li X H and Sun R 2015 *Chin. Phys. B* **24** 114204

[12] Zhang M, Wang J H, Jin W, Huang Z H and Kobayashi H 2015 *Combust. Flame* **162** 2087

[13] Fu J, Tang C L, Jin W and Huang Z H 2014 *Int. J. Hydrogen Energ.* **39** 12187

[14] Fu J, Leung C W, Huang Z H, Zhang Y and Cheung C S 2016 *Exp. Therm. Fluid* **70** 335

[15] Holthuis 2015 "Associates, Flat Flame Burners", http://www.flatflame.com

[16] Weigand P, Lückerath R, Meier W 2003 "Documentation of flat premixed laminar CH_4/air standard flames: Temperatures and species concentrations", http:// www. dlr. de/ VT/ Datenarchiv

[17] Giezendanner-Thoben R, Meier U, Meier W, Heinze J and Aigner M 2005 *Appl. Opt.* **44** 6565

[18] Goldman A and Gillis J R 1981 *J. Quantum Spectrosc. Radiat. Transfer* **25** 111

[19] Luque J and Crosley D R 1999 Lifbase: database and spectral simulation program (version 1.5), SRI international report MP 99-009

[20] Chen S, Su T, Zheng Y B, Chen L, Liu T X, Li R B and Yang F R 2016 *Chin. Phys. B* **25** 060703

[21] Kee R J, Grcar J F, Smooke M D, Miller J A and Meeks E 1985 PREMIX: a Fortran program for modeling steady laminar one-dimensional premixed flames, Sandia National Laboratories Report